J Supercond Nov Magn (2016) 29:253–263
DOI 10.1007/s10948-015-3249-5

ORIGINAL PAPER

Magneto-Optical and Catalytic Properties of Recyclable Spinel $NiAl_2O_4$ Nanostructures Using Facile Combustion Methods

S. Jayasree[1,2] · A. Manikandan[3] · S. Arul Antony[4] · A. M. Uduman Mohideen[2] · C. Barathiraja[5]

Received: 7 August 2015 / Accepted: 26 September 2015 / Published online: 14 October 2015

Abstract Spinel nickel aluminate ($NiAl_2O_4$) nanospheres (NSPs) and nanoplatelets (NPLs) were successfully synthesized using a facile microwave combustion method (MCM) and conventional combustion method (CCM), respectively, using urea as the fuel. The as-prepared samples were characterized by powder X-ray diffraction (XRD), Fourier transform infrared (FT-IR), high-resolution scanning electron microscopy (HR-SEM), high-resolution transmission electron microscopy (HR-TEM), energy-dispersive X-ray spectroscopy (EDX), selected area electron diffraction (SAED), UV–Visible diffuse reflectance spectroscopy (DRS), photoluminescence (PL) spectroscopy, and vibrating sample magnetometer (VSM) analysis. Powder XRD, FT-IR, EDX, and SAED results showed that the samples were pure phase spinel $NiAl_2O_4$ nanocrystals without any other secondary phase impurity. UV–Vis DRS and PL spectroscopy results were used to calculate the energy band gap (E_g) value of the samples which is 3.41 and 3.08 eV for $NiAl_2O_4$ NSPs and $NiAl_2O_4$ NPLs, respectively. VSM results of the $NiAl_2O_4$ NPLs sample show lower M_s (49.16×10^{-3} emu/g) values compared with the $NiAl_2O_4$ NSPs sample (73.42×10^{-3} emu/g), which confirm that both the products have ferromagnetic behavior. $NiAl_2O_4$ NSPs were found to have higher surface area than $NiAl_2O_4$ NPLs, which in turn leads to the improved performance towards the selective oxidation of benzyl alcohol into benzaldehyde, with 100 % selectivity, and it was found that the $NiAl_2O_4$ NSPs sample show higher conversion (96.25 %) than $NiAl_2O_4$ NPLs (85.37 %). The as-prepared samples show high activity, good reusability, remarkable stability, and environmentally friendly materials for industrial and technological applications.

Keywords Nanocrystals · Spinel $NiAl_2O_4$ · Microwave combustion · Opto-magnetic properties · Catalytic properties

✉ A Manikandan
mkavath15@gmail.com;
manikandana.che@bharathuniv.ac.in

✉ A. M. Uduman Mohideen
amuduman14@gmail.com

[1] Department of Chemistry, Kunthavai Naacchiyaar Government Arts College for Women (Autonomous), Thanjavur 613007, Tamil Nadu, India

[2] Postgraduate and Research Department of Chemistry, Khadir Mohideen College, Adirampattinam, Thanjavur 614701, Tamil Nadu, India

[3] Department of Chemistry, Bharath Institute of Higher Education and Research, Bharath University, Chennai 600073, Tamil Nadu, India

[4] Postgraduate and Research Department of Chemistry, Presidency College (Autonomous), Chennai 600005, Tamil Nadu, India

[5] Department of Chemistry, Mannai Rajagopalaswami Government Arts College Mannargudi 614001 Tamil Nadu, India

1 Introduction

Nowadays, nanostructured spinel type mixed metal oxides have attracted significant attention in many areas such as

ceramics, semiconductors, sensors and catalytic materials [1–6]. Among them, spinel aluminates have high thermal stability, hydrophobicity, high mechanical resistance, and low surface acidity [7–13]. Nanocrystalline spinel aluminates with the general formula AB_2O_4, where A^{2+} (tetrahedral) and B^{3+} (octahedral) are divalent (Ni^{2+}, Cu^{2+}, Co^{2+}, etc.) and trivalent (Al^{3+}) cations, respectively, attract the research interest, because of their versatile practical applications. Over the spinel metal aluminates, nickel aluminate ($NiAl_2O_4$) have been studied for many applications, including magnetic materials, pigments, catalysts, and refractory materials, which belong to the space group *Fd3m* [14, 15]. $NiAl_2O_4$ nanostructures have unique properties such as structural, morphological, optical, electrical, magnetic and catalytic activities compared with bulk materials, due to their smaller particle size and higher surface area. Its remarkable electrical and magnetic properties depend upon the nature of the ion distribution among A and B sites [16]. $NiAl_2O_4$ is an inverse spinel in which half of the Al^{3+} ions preferentially fill the A sites and the other occupies the B sites. Thus, the spinel $NiAl_2O_4$ can be represented by the formula $(Al^{3+})_A(Ni^{2+}Al^{3+})_BO_4^{2-}$ [17, 18].

It is well known that nanoparticles with controlled size and composition have fundamental and technological interest in nanoscience and nanotechnology. Spinel $NiAl_2O_4$ nanostructures have been prepared using several methods, such as solid-state reaction, solgel, co-precipitation, hydrothermal solvothermal methods [19–24], etc. Spinel-type mixed metal oxides are usually prepared using a ceramic technique, which involves high-temperature solid-state reactions that resulted to large and non-uniform size particles [25]. Nowadays, many researchers have been used the combustion synthesis for the preparation of a variety of advanced ceramics, catalysts and nanomaterials. Moreover, microwave combustion method (MCM) offers great advantages such as prompting the rapid reaction due to the molecular level interaction of the microwave radiations with the reactant species. Also, MCM route is an easy and convenient one than the above mentioned methods. Moreover, it produces the homogeneous distribution of nanostructures at lower temperatures without further calcinations and also shorter reaction times, when compared with the above methods [26].

The advantage of the MCM technique is the dispersion of the raw materials in liquid precursors, which produced the crystallized nanopowders with smaller particle size and high-purity products with large scale [27]. It is a clean, cheap, and convenient route, which results in uniform particle morphology and shorter reaction time and is also a promising method for the preparation of various nanostructured materials with different sizes and shapes. Moreover, it is environmentally friendly, simple to operate and energy efficient over the conventional methods [28], due to the yields of the final products of metal oxides associated with their special structural personalities, namely nano-sized dimensions. Besides, to our knowledge, no literature is available on the magneto-optical properties of spinel $NiAl_2O_4$ nanostructures using a simple microwave combustion method using urea as the fuel for the applications of catalytic oxidation of benzyl alcohol into benzaldehyde.

Spinel $NiAl_2O_4$ nanostructures have received much attention as a catalyst, due to its stability and reusability, and it can be recovered easily from the reaction mixture using a simple filtration method [29]. It is well known that the catalytic activity of the ceramic materials depends on grain size and surface area, making it suitable for catalyst support [30]. Moreover, spinel $NiAl_2O_4$ is non-toxic, inexpensive, and relatively high surface area making them fit for use as a cost-effectively and eco-friendly viable solid heterogeneous catalyst. The as-prepared spinel $NiAl_2O_4$ nanostructures were investigated for structural, morphological, optical, magnetic, and catalytic properties, and different characterizations have been carried out using powder X-ray diffraction (XRD), Fourier transform infrared (FT-IR), high-resolution scanning electron microscopy (HR-SEM), high-resolution transmission electron microscopy (HR-TEM), energy-dispersive X-ray spectroscopy (EDX), Brunauer–Emmett–Teller (BET), UV–Visible diffuse reflectance spectroscopy (DRS), photoluminescence (PL) spectroscopy, and vibrating sample magnetometer (VSM) techniques, and the obtained results are presented here.

2 Experimental Part

2.1 Preparation of Spinel $NiAl_2O_4$ Nanostructures Using Microwave Combustion Method and Conventional Combustion Method

All the chemicals used in this study were of analytical grade obtained from Merck, India, and were used as received without further purification. All chemicals such as nitrates of nickel and aluminum and urea were used as the fuel for this method. The stoichiometry of metal nitrate salts and fuel was calculated based on the total oxidizing and reducing valences related to the oxidant agents and to the fuels. Initially, the precursor mixture of nitrate solution in urea was placed in a domestic microwave oven and exposed to the microwave energy in a 2.45-GHz multimode cavity at 850 W for 10 min. When the solution attained the point of spontaneous combustion, ignition took place, resulting in a rapid flame and yielding solid fluffy final products. The obtained solid powders were washed well with water and ethanol several times and dried at 80 °C for 1 h and labeled as $NiAl_2O_4$ nanospheres (NSPs) and then used for further characterizations.

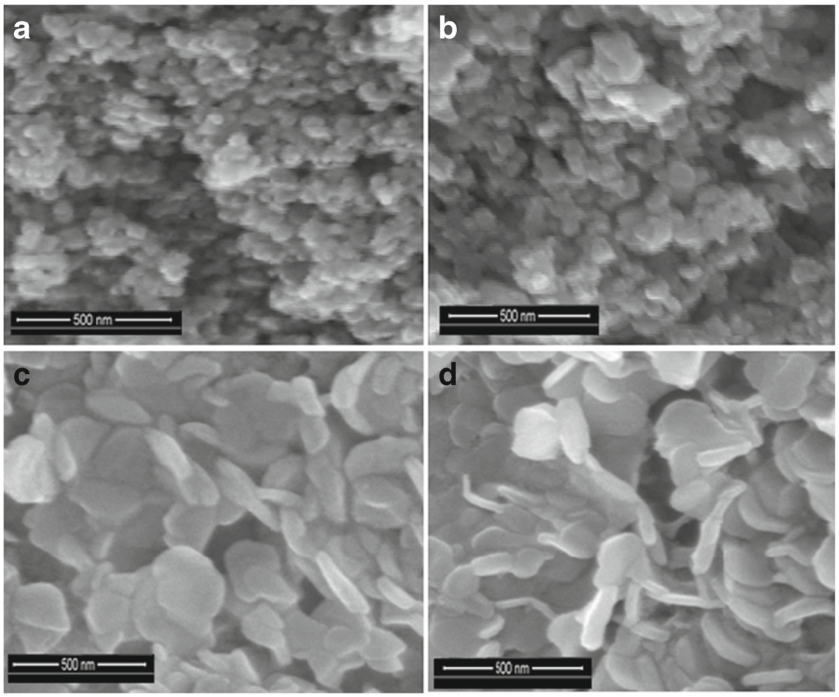

Fig. 1 HR-SEM images of $NiAl_2O_4$ NSPs (**a**, **b**) and $NiAl_2O_4$ NPLs (**c**, **d**) samples

In the next separate experiment, conventional combustion method (CCM), the same reaction mixture was taken in the silica crucible and treated in an air furnace at 500 °C for 2 h at a heating rate of 5 °C/min and cooled at the same rate; it became solid, which was labeled as $NiAl_2O_4$ nanoplatelets (NPLs).

2.2 Characterizations of Spinel $NiAl_2O_4$ Nanostructures

The structural characterization of spinel $NiAl_2O_4$ nanostructures was performed using a Philips X'Pert X-ray diffractometer with CuKα radiation at $\lambda = 1.540$ Å. The surface functional groups were analyzed using a PerkinElmer FT-IR spectrometer. Morphological studies and energy-dispersive X-ray analysis of spinel $NiAl_2O_4$ samples have been performed with a JEOL JSM6360 high-resolution scanning electron microscope. The transmission electron micrographs were carried out by Philips CM20 TEM. The surface area was derived from the N_2 adsorption–desorption isotherms using liquid nitrogen at 77 K using an automatic adsorption instrument (Nova 1000 gas sorption analyzer; Quantachrome Corp.). The UV–visible diffuse reflectance spectrum of spinel $NiAl_2O_4$ samples was recorded using a Cary 100 UV–visible spectrophotometer to estimate their energy band gap (E_g). The photoluminescence properties were recorded at room temperature using a Varian Cary Eclipse Fluorescence Spectrophotometer. The magnetic properties were investigated at room temperature in an applied magnetic field sweeping from −10 to +10 KOe using a PMC MicroMag 3900 model vibrating sample magnetometer (VSM) equipped with a 1-T magnet.

2.3 Catalytic Test

The oxidation of benzyl alcohol using spinel $NiAl_2O_4$ nanocatalysts was carried out in a batch reactor operated under atmospheric conditions. Five micromolars of the oxidant (H_2O_2) was added along with 0.5 g of nano-sized $NiAl_2O_4$ catalysts ($NiAl_2O_4$ NSPs and $NiAl_2O_4$ NPLs), and the contents were heated at 80 °C in an acetonitrile medium for 5 h in a three-neck round-bottom flask equipped with a reflux condenser and thermometer. The oxidized products after the catalytic reaction are collected and studied using an Agilent GC spectrometer. The column used for the study was DB wax column (capillary column) with a length of 30 mm, and helium was used as the carrier gas. GC technique was carried out to know the conversion percentage of the products.

3 Results and Discussion

3.1 Scanning Electron Microscopy Studies

The surface morphology of the samples was investigated by high resolution scanning electron microscopy (HR-SEM) analysis. The HR-SEM images of $NiAl_2O_4$ nanospheres (NSPs) prepared using the MCM route are shown in Fig. 1a,

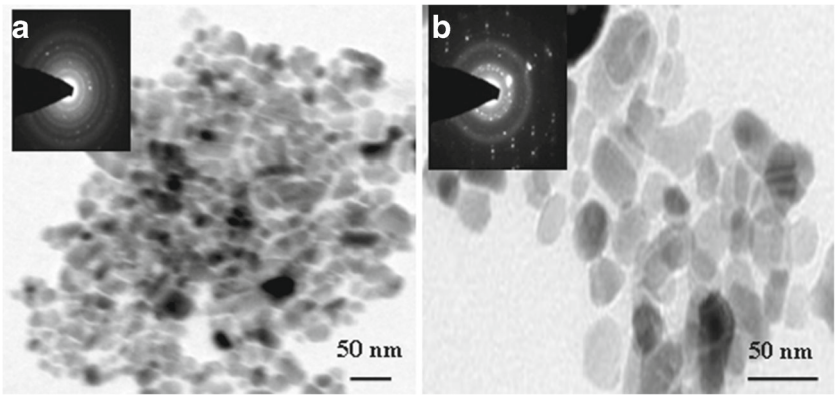

Fig. 2 HR-TEM images of $NiAl_2O_4$ NSPs (**a**) and $NiAl_2O_4$ NPLs (**b**) samples. The *insets* of **a**, **b** are the corresponding SAED pattern of the samples

b, which confirm the presence of NSPs like particle morphology with agglomeration. Therefore, we could infer that the spinel $NiAl_2O_4$ NSPs was formed in the MCM route. It reveals that the NSPs are homogeneous and grains are distributed uniformly with smaller size and large agglomerates with a diameter below 10 nm, due to the fact that the MCM route is a volumetric and uniform heating method, when compared to the CCM route, which is a non-uniform and radiative method. Within the limited time, nucleation and growth had to be finished using the MCM route; hence, the particles with smaller and narrow distribution were obtained.

Figure 1c, d shows the HR-SEM images of $NiAl_2O_4$ NPLs prepared using the CCM route, which confirm the formation of nanoplatelets (NPLs) like morphology with agglomeration. In the CCM, the reaction was completed only after 2 h, whereas in the MCM, the reaction was completed within few minutes of time. However, in the CCM, the time might be sufficient to form the separate phases, which has led to the bigger particle size of 20 nm with wider distribution, but in the MCM route, the size of the particle is only below 10 nm. Therefore, we can infer that the agglomerated $NiAl_2O_4$ NSPs and $NiAl_2O_4$ NPLs formed during the MCM and CCM approaches, respectively. Thus, the higher temperature and non-uniform heating method of CCM reaction in a furnace caused the grain growth than the MCM route. Moreover, the $NiAl_2O_4$ NPLs sample is exposed for more time, and it results in the formation of agglomeration (may be due to the sintering effect). However, the morphology of the final products depends on the preparation methods and temperatures.

3.2 Transmission Electron Microscopy Studies

In order to further confirm the morphology and particle size of the samples, high resolution transmission electron microscopy (HR-TEM) studies are carried out. Figure 2a shows the HR-TEM image of the spinel $NiAl_2O_4$ sample prepared using the MCM route, which confirms the formation of NSPs like particle morphology with smaller size. The obtained particles are nearly spherical in shape with a uniform size distribution for the $NiAl_2O_4$ NSPs sample. The average size and void space diameter of single $NiAl_2O_4$ NSPs are found to be in the range of 7–10 nm. It may be due to the fact that spinel $NiAl_2O_4$ was prepared within a short reaction time of 10 min by means of a domestic microwave oven operated at 2.45 GHz (850 W).

The image of spinel $NiAl_2O_4$ NPLs like particles with bigger particle size for the $NiAl_2O_4$ NPLs sample prepared using the CCM route is shown in Fig. 2b, which confirms the formation of NPLs like particle morphology with a diameter range of 18–22 nm in size. Moreover, the nanoparticles prepared under MCM route were of narrower distribution than those prepared using the CCM approach. It is concluded that the temperature is a key factor in the controlled synthesis of nano-sized materials. Herein, spinel $NiAl_2O_4$ NSPs and $NiAl_2O_4$ NPLs like particles were prepared by the temperature optimization only and there is no use of any other solvent, surfactant, and catalyst. Also, the mean particle size determined by HR-TEM analysis is very close to the average crystallite size calculated using the Scherrer formula from the powder X-ray diffraction (XRD) pattern, which is reported later in Section 3.4. The crystallinity and crystalline nature of the samples were confirmed by selected area electron diffraction (SAED) pattern. The SAED pattern of the spinel $NiAl_2O_4$ NSPs and $NiAl_2O_4$ NPLs is shown in Fig. 2a, b (insets), respectively. The SAED pattern implies that the prepared samples are good crystalline materials with higher crystalline nature.

3.3 Energy-Dispersive X-ray Analysis

The purity and elemental compositions of the samples were confirmed by means of energy dispersive X-ray spectroscopy (EDX) analysis. Figure 3a b shows the EDX spectra of $NiAl_2O_4$ NSPs and $NiAl_2O_4$ NPLs, respectively. It exhibited Ni, Al, and O peaks and indicated the presence

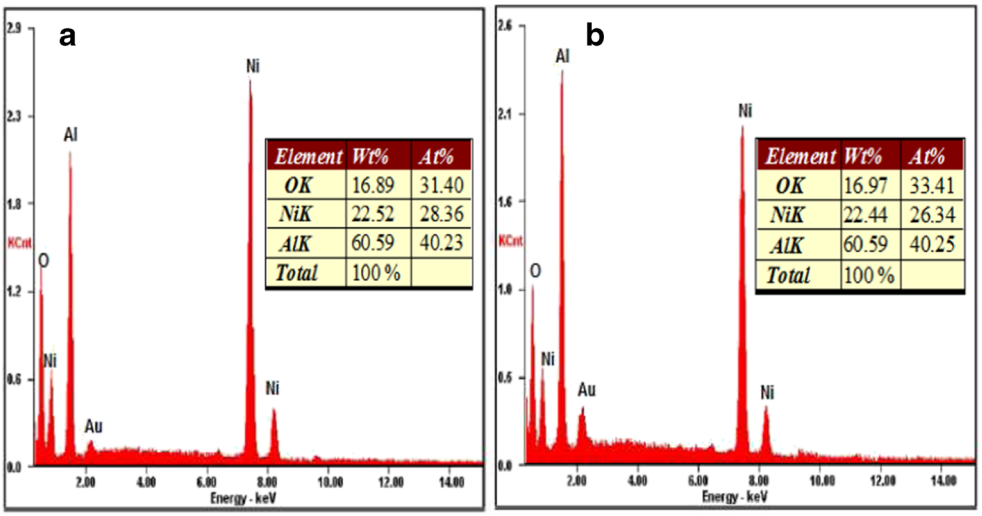

Fig. 3 EDX spectrum of $NiAl_2O_4$ NSPs (**a**) and $NiAl_2O_4$ NPLs (**b**) samples

of $NiAl_2O_4$ phase without any other impurity. In the EDX pattern, the presence of Al, Ni, and O elements in proper proportions suggested that the expected stoichiometry was maintained in the prepared samples. It is in good agreement with the powder XRD analysis, which is reported later in Section 3.4. The peak at 2.1 KeV in the EDX spectra were due to the gold coated samples before HR-SEM recording for better visibility of the surface morphology

3.4 Powder X-ray Diffraction Analysis

The powder XRD pattern of the prepared samples is given in Fig. 4. Figure 4a b shows the powder XRD pattern of the $NiAl_2O_4$ NSPs (prepared using the MCM) and $NiAl_2O_4$ NPLs (prepared using the CCM) samples respectively using urea as the fuel It revealed that both the $NiAl_2O_4$ NSPs and $NiAl_2O_4$ NPLs samples had higher crystalline nature The diffraction peaks at 2θ values of 31.27, 37.04, 38.87, 45.06, 49.26, 55.73, 59.38, 65.43, 74.28 and 77.51 correspond to (220), (311), (222), (400), (331), (422), (511), (440), (620), and (533) planes, respectively, which can be readily assigned to a cubic phase of spinel $NiAl_2O_4$ (space group Fd3m). The diffraction peaks of the samples matched well with the JCPDS card no. 10-0339 [31]. No characteristic peak related to any other secondary phase impurity was observed. Further observation revealed that both the samples had sharp peaks indicating good crystallinity, but the diffraction peaks of the $NiAl_2O_4$ NSPs sample were slightly broadened compared with $NiAl_2O_4$ NPLs due to the smaller crystallite size. The average crystallite size for both the samples was calculated using the Scherrer formula.

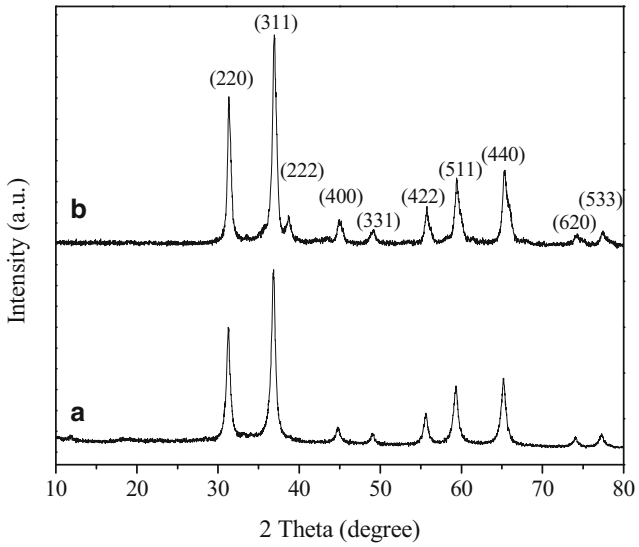

Fig. 4 Powder XRD pattern of $NiAl_2O_4$ NSPs (**a**) and $NiAl_2O_4$ NPLs (**b**) samples

$$L = \frac{0.89\lambda}{\beta \cos\theta} \quad (1)$$

where L is the average crystallite size (nm), λ is the X-ray wavelength (0.154 nm), θ is the diffraction angle and β is the full width at half maximum of the observed peaks. The average crystallite size for both the $NiAl_2O_4$ NSPs and $NiAl_2O_4$ NPLs samples was found to be 7.92 and 21.45 nm, respectively. The average crystallite size of the $NiAl_2O_4$ NSPs sample is lower than that of the $NiAl_2O_4$ NPLs sample, which are calculated from the full width at half maximum of the (311) plane. The observed higher crystallite size of $NiAl_2O_4$ NPLs (prepared using the CCM route) is due to the high-temperature calcinations (500 °C for 2 h) compared with the $NiAl_2O_4$ NSPs sample prepared using the MCM route [32]. However, the MCM approach produces spinel $NiAl_2O_4$ NSPs in a microwave oven operated at a power of 850 W and a temperature ranging from 150 to 400 °C that would result to the formation of final products

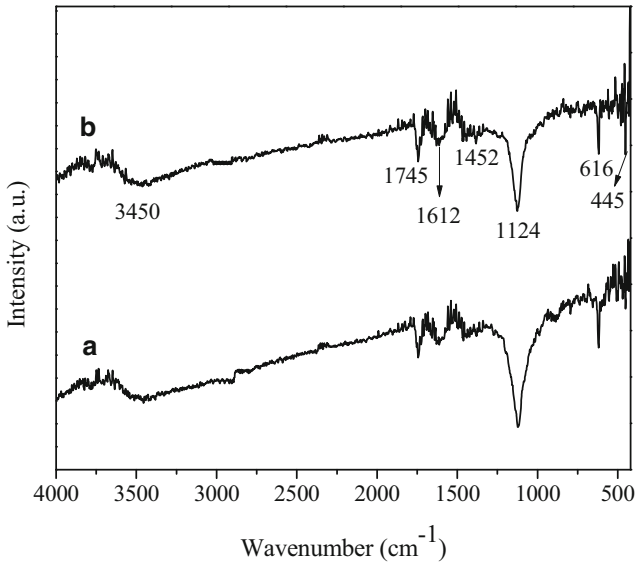

Fig. 5 FT-IR spectra of $NiAl_2O_4$ NSPs (**a**) and $NiAl_2O_4$ NPLs (**b**) samples

within 10 min with smaller crystallite size. Compared with the CCM, MCM is more time saving and higher in production scale. Also, the broad reflection peaks of the $NiAl_2O_4$ NSPs sample proved very fine crystallite size prepared using the MCM route. However, when heat treatment in the CCM route was increased, the diffraction lines become narrower and more intense, resulting in higher crystallite size ($NiAl_2O_4$ NPLs), which can be further understood by heat treatment at higher temperature (500 °C) to enhance the crystallite size of spinel $NiAl_2O_4$ [33].

3.5 Fourier Transform Infrared Analysis

The Fourier transform infrared (FT-IR) spectral analysis has been used to study the functional groups of the samples. Figure 5a and b shows the FT-IR spectra of $NiAl_2O_4$ NSPs and $NiAl_2O_4$ NPLs samples prepared using both CCM and MCM, respectively and exhibits a broad band near 3450 cm^{-1}, due to the –OH stretching vibration, and a second typical absorption band at 1612 cm^{-1} is assigned to the deformative vibration of H_2O molecules, which is most probably, due to the H_2O absorption when making the samples by pellets with KBr [34]. The metal–oxygen (Ni–O, Al–O and Ni–O–Al) stretching frequencies were observed in the range 450–650 cm^{-1}, which are associated with the vibrations of Al–O, Ni–O and Ni–O–Al bonds. The characteristic of metal–oxygen frequencies present in the molecule indicates the formation of single-phase spinel $NiAl_2O_4$ [35]. The absorption at 1452 and 1124 cm^{-1} corresponds to the vibration mode of Al–OH and Ni–OH, which are typical of this class of materials. In addition, a strong band at 1745 cm^{-1} is essential due to OH– vibration modes of hydrogen bonded –OH. No other impurity phase was detected by FT-IR spectra, and it was in good agreement with the results obtained by powder XRD analysis

3.6 UV–Visible Diffuse Reflectance Spectroscopy Analysis

The optical band gap and the electronic structures of the metal oxide semiconductor materials were determined by UV–Visible absorption/reflectance/transmittance analysis. UV–Visible diffuse reflectance spectroscopy (DRS) studies play a vital role in estimating the energy band gap (E_g) of the metal oxide semiconductors. The optical band gap was calculated using Tauc relation [36]. The Kubelka–Munk function is generally applied to convert the DRS into equivalent absorption coefficient and mostly used for analyzing the powder samples [37]. The Kubelka–Munk function $F(R)$ was used to calculate the E_g of the spinel $NiAl_2O_4$ semiconductors. Thus, the vertical axis is converted into quantity $F(R)$ which is equal to the absorption coefficient. Thus, the α in the Tauc equation is substituted with $F(R)$ and, hence, the relation becomes

$$(F(R)) = \alpha = \frac{(1-R)^2}{2R} \tag{2}$$

where $F(R)$ is the Kubelka–Munk function, α is the absorption coefficient, and R is the reflectance. Thus the Tauc relation becomes

$$F(R)\,h\upsilon = A\left(h\upsilon - E_g\right)^n \tag{3}$$

where $n = 0.5$ and 2 for direct and indirect transitions, respectively, thus giving direct and indirect band gaps. The plots of $(F(R)\,h\upsilon)^2$ versus $h\upsilon$ for both samples are shown in Fig. 6. Extrapolation of linear regions of these plots to $(F(R)\,h\upsilon)^2 = 0$ gives the direct band gap values. The

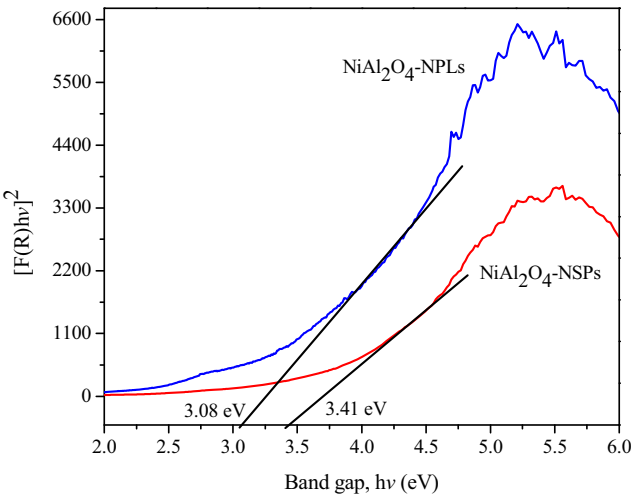

Fig. 6 UV–Vis. DRS study of $NiAl_2O_4$ NSPs and $NiAl_2O_4$ NPLs samples

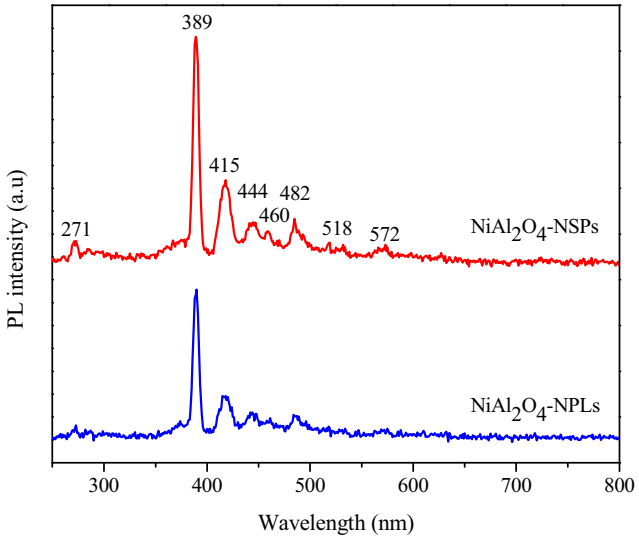

Fig. 7 Room-temperature PL spectra of $NiAl_2O_4$ NSPs and $NiAl_2O_4$ NPLs samples

direct band gap (E_g) value of the $NiAl_2O_4$ NSPs sample was observed to be 3.41 eV, and it is decreased with increasing the higher crystallite size of the $NiAl_2O_4$ NPLs sample (3.08 eV). The observed higher E_g value of the $NiAl_2O_4$ NSPs sample is due to smaller particle size. Interestingly, the energy band gap decreased with increasing the crystallite size of the samples, which obeys the quantum confinement effect

3.7 Photoluminescence Spectroscopy

Room-temperature photoluminescence (PL) spectroscopy gives the information about the band gap with the relative active position of sub-band gap and defect states of the metal oxide semiconductors [38, 39], and it is an important tool for investigating the electronic and optical properties of the semiconducting materials. Figure 7 demonstrates the room-temperature PL spectra recorded at $\lambda_{ex} = 265$ nm of $NiAl_2O_4$ samples prepared using the two different methods namely MCM and CCM, respectively. A small band observed at 271 nm (4.57 eV) is ascribed to the near-band edge (NBE) emission of the wide band gap of $NiAl_2O_4$ due to the recombination of free excitons through an exciton–exciton process. The estimated band gap (3.39 eV) from the NBE emission is in agreement with the band gap estimated from the Kubelka–Munk plot derived from the UV–Visible DRS spectra. However, both the samples show a sharp peak at 389 nm (3.18 eV) which may be ascribed to the oxygen vacancies. Violet emissions centered at 415 nm (2.98 eV) and 444 nm (2.79 eV), due to the radiating defects related to the interface traps existing at the grain boundaries.

Also, blue emissions appeared at 460 nm (2.69 eV) and 482 nm (2.57 eV), which represent a deep level of visible emissions associated with localized levels in the band gap [40, 41]. Green emission centered at 518 nm (2.39 eV) and 572 nm (2.16 eV) may be ascribed to the oxygen vacancies. It is found from the room-temperature PL spectra that the emission characteristics are governed by the defect-controlled processes. The $NiAl_2O_4$ NSPs sample shows the higher intensity and may exhibit greater catalytic activity than $NiAl_2O_4$ NSPs.

3.8 Vibrating Sample Magnetometer Measurements

Magnetic properties of the samples have been analyzed by room-temperature vibrating sample magnetometer (VSM) analysis. Figure 8 shows the magnetic hysteresis loop of the spinel $NiAl_2O_4$ NSPs and $NiAl_2O_4$ NPLs, prepared using MCM and CCM approaches, respectively. The shape and the area of the M–H hysteresis loops were found to depend

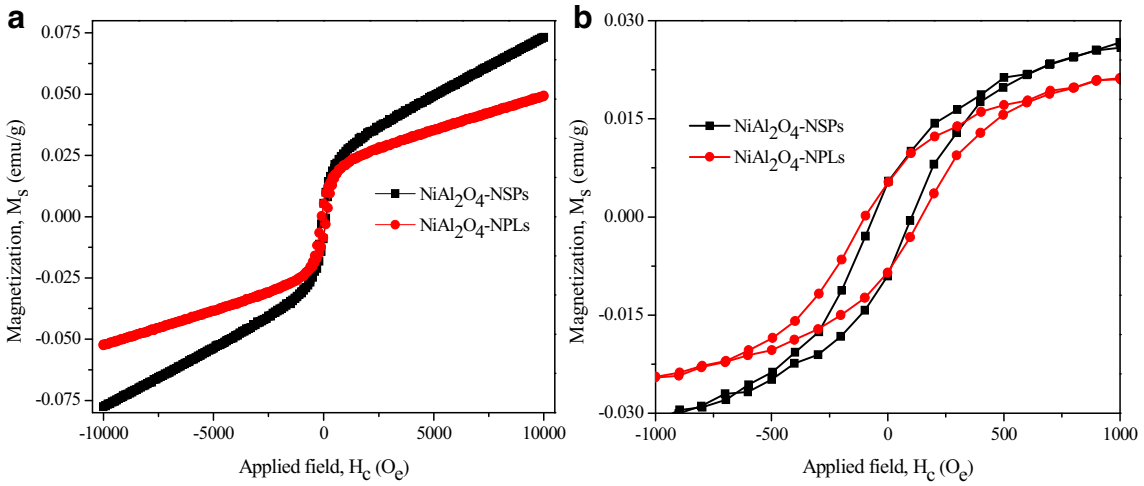

Fig. 8 **a**, **b** Magnetic hysteresis (M–H) loop of $NiAl_2O_4$ NSPs and $NiAl_2O_4$ NPLs samples

Table 1 Crystallite size, magnetic parameters [magnetization (M_s), coercivity (H_c), and remanent magnetization (M_r)], surface area, conversion and selectivity percentage for the oxidation of benzyl alcohol into benzaldehyde

Samples	Crystallite size (nm)	H_c (O_e)	$M_r \times 10^{-3}$ (emu/g)	$M_s \times 10^{-3}$ (emu/g)	BET surface area (m^2/g)	Conversion (%)	Selectivity (%)
$NiAl_2O_4$ NSPs	7.65	64.75	4.827	73.42	86.77	96.25	100
$NiAl_2O_4$ NPLs	19.82	98.25	5.336	49.16	69.85	85.37	100

strongly on the preparation methods as well as on the ratio of the crystalline phases in the powders. Both the samples displayed the normal (s-shaped) narrow hysteresis loops, and the magnetic parameters like saturation magnetization (M_s), remanent magnetization (M_r), and coercivity (H_c) of the samples are summarized in Table 1. The shape of the $M-H$ hysteresis loop shows a characteristic weak ferromagnetic behavior for both samples. From the VSM measurements, the H_c and the M_r are estimated to be 64.75 O_e and 4.827 $\times$ 10^{-3} emu/g for the $NiAl_2O_4$ NSPs sample, respectively, and 98.25 O_e and 5.336 $\times$ 10^{-3} emu/g for the $NiAl_2O_4$ NPLs sample, respectively. The M_s of the $NiAl_2O_4$ NSPs sample (73.42 $\times$ 10^{-3} emu/g) is higher than that of the $NiAl_2O_4$ NPLs sample (49.16 $\times$ 10^{-3} emu/g), and both the samples are weak ferromagnetic in nature. The lower H_c and M_r values confirm that the spinel $NiAl_2O_4$ NSPs and $NiAl_2O_4$ NPLs samples have soft and weak ferromagnetic nature.

Spinel $NiAl_2O_4$ nanocrystals have inverse spinel structure with the ferromagnetic nature, due to the exchange between the ions occupying the tetrahedral (A) and octahedral (B) sites. Also, it has zero net magnetization, because of the complete compensation of the sublattice magnetization [42, 43]. At room temperature, the H_c values of the $NiAl_2O_4$ NPLs sample is 98.25 O_e, which is higher than the $NiAl_2O_4$ NSPs sample (64.75 O_e), and it is probably attributed to the high shape anisotropy of spinel $NiAl_2O_4$ nanocrystals, which allow them in magnetizing in all directions along their easy magnetic axes. As a result, the different M_s values of spinel $NiAl_2O_4$ NSPs and $NiAl_2O_4$ NPLs samples prepared using MCM and CCM, respectively, could be related to the change in the sizes of the particles. It is well known that the magnetic property of nanomaterials is strongly dependent on the shape and sizes of the particles and their crystallinity. However, it is observed that the lower H_c and M_r values confirm that the $NiAl_2O_4$ NSPs and $NiAl_2O_4$ NPLs samples have soft and weak ferromagnetic nature [43]

3.9 Catalytic Tests

The catalytic performance of $NiAl_2O_4$ NSPs and $NiAl_2O_4$ NPLs samples prepared using MCM and CCM, respectively, was evaluated in the oxidation of benzyl alcohol in the presence of 30 % H_2O_2 as oxidant. In the catalytic oxidation reaction, benzyl alcohols (5 mmol) and H_2O_2 (5 mmol) as the oxidant were added with 0.5 g of heterogeneous catalyst ($NiAl_2O_4$ NSPs or $NiAl_2O_4$ NPLs) and the contents were heated at 80 °C in the presence of acetonitrile (5 mmol) as the solvent for 5 h. Catalytic conversion and product selectivity strongly depend on the particle size and surface area of the catalyst which was confirmed by catalytic analysis. The observed catalytic results are summarized in Table 1. The resultant catalysts prepared using the two different methods display clear difference in the selective oxidation of benzyl alcohol into benzaldehyde with 100 % selectivity

3.9.1 Effects of Surface Area

Generally, a high specific surface area has a favorable effect on the activity for heterogeneous catalysis. In order to have an idea of the adsorbance capability of spinel $NiAl_2O_4$ NSPs and $NiAl_2O_4$ NPLs, BET surface area was determined using N_2 adsorption–desorption studies and the observed values are given in Table 1. The surface area of the $NiAl_2O_4$ NSPs sample was found to be higher, i.e., 86.77 m^2/g, than that of the $NiAl_2O_4$ NPLs sample (69.85 m^2/g), and the observed difference may be due to the smaller particle size of $NiAl_2O_4$ NSPs compared with $NiAl_2O_4$ NPLs, which is confirmed by HR-SEM and HR-TEM analysis. In this present study, the surface area parameters of the samples varied according to the preparation method. Moreover, it is believed that the high surface area of $NiAl_2O_4$ NSPs could enhance the catalytic activity than the lower surface area of the $NiAl_2O_4$ NPLs sample. The surface area of $NiAl_2O_4$ NSPs and $NiAl_2O_4$ NPLs samples is 86.77 and 69.85 m^2/g, respectively. It was found that the conversion of benzyl alcohol into benzaldehyde for the $NiAl_2O_4$ NSPs sample was higher than that of $NiAl_2O_4$ NPLs (Fig. 9). It is mainly due to the uniform distribution with smaller particle size of $NiAl_2O_4$ NSPs catalyst. The oxidation of benzyl alcohol into benzaldehyde was achieved with 96.25 % conversion and 100 % selectivity of benzaldehyde using the $NiAl_2O_4$ NSPs catalyst, which has higher conversion compared with $NiAl_2O_4$ NPLs (86.54 %

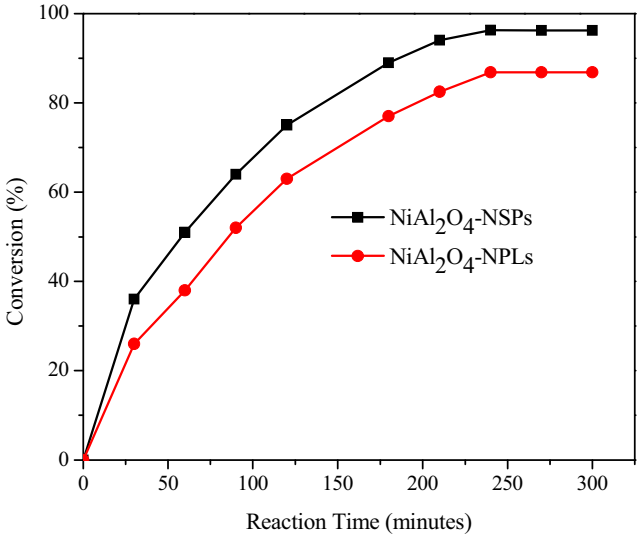

Fig. 9 The catalytic reaction time of $NiAl_2O_4$ NSPs and $NiAl_2O_4$ NPLs samples on the conversion towards the oxidation of benzyl alcohol into benzaldehyde (reaction conditions: catalyst 0.5 g; benzyl alcohol, 5 mmol; acetonitrile, 5 mmol; H_2O_2, 5 mmol; temperature, 80 °C; time, 5 h)

conversion with 100 % selectivity). The observed higher efficiency of $NiAl_2O_4$ NSPs catalyst in this oxidation reaction can be attributed to the high dispersity, and large surface area provides more catalytic active sites for this reaction [44]. High specific surface area of $NiAl_2O_4$ NSPs (86.77 m^2/g) was useful to catalytic activity via enhancing the adsorption of benzyl alcohol through the surface of the catalyst and is the determining step in the catalytic reaction [45]. However, the $NiAl_2O_4$ NPLs sample shows poor performance, due to the larger particle size with lower surface area (6985 m^2/g). In the MCM approach, the final product is formed within few minutes of time with homogeneous and smaller particle size with higher surface area, which enhances their catalytic activity compared with $NiAl_2O_4$ NPLs. In addition, when the surface area increases, the amount of the dispersion of particles per volume in the solution will increase and this enhanced the catalytic activity.

3.9.2 Effect of Reaction Time

Catalytic reaction time is very important to measure the activity of catalyst. Figure 9 shows the effect of reaction time on the conversion of benzyl alcohol into benzaldehyde using a heterogeneous ($NiAl_2O_4$ NSPs and $NiAl_2O_4$ NPLs) catalyst. It was found that the conversion increased linearly by increasing the reaction time up to 180 min and then increasing it slowly from 180 to 240 min. The product conversion was found to be nearly the same for the 240- and 300-min experiments, indicating the constant conversion after 240 min. No significant change in the oxidation of benzyl alcohol into benzaldehyde was observed when running the reaction for 300 min [46]. However, the catalytic activity of the $NiAl_2O_4$ NSPs sample is higher than that of the $NiAl_2O_4$ NPLs sample, due to the smaller particle size distribution which would be a potentially efficient catalyst [47].

3.9.3 Effect of Catalyst Amount

The influence of the catalyst amount on the conversion towards the oxidation of benzyl alcohol into benzaldehyde is shown in Fig. 10. The conversion is gradually increased with increase in the amount of catalyst from 0.1 to 0.5 g, (reaction conditions: catalyst, 0.1 to 0.8 g; benzyl alcohol, 5 mmol; acetonitrile, 5 mmol; H_2O_2, 5 mmol; temperature, 80 °C; time, 5 h), and further increasing the catalyst amount (0.6 to 0.8 g), the conversion and yield remain nearly the same, which suggests that a large amount of catalyst is not needed to improve the reaction product [46]. However, it is found that with the increase of catalyst amount, the conversion and yield increased up to 0.5 g and this may be apparently due to the availability of more catalytic active sites of the catalyst.

3.9.4 Reusability Studies

The catalytic oxidation of benzyl alcohol into benzaldehyde was employed as a model reaction to investigate the reusability of spinel $NiAl_2O_4$ NSPs and $NiAl_2O_4$ NPLs catalysts. The recycling of the catalyst is very important for industrial and technological applications for reusability of

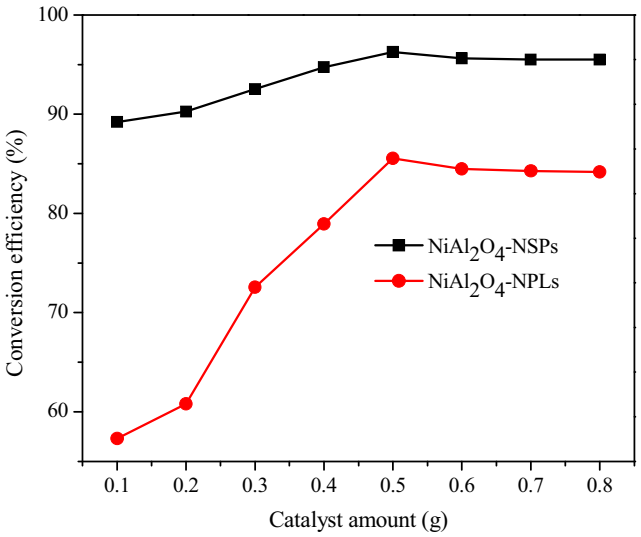

Fig. 10 **a**, **b** The amount of spinel catalysts of $NiAl_2O_4$ NSPs and $NiAl_2O_4$ NPLs samples on the conversion towards the oxidation of benzyl alcohol into benzaldehyde (reaction conditions: catalyst 0.1 to 0.8 g; benzyl alcohol, 5 mmol; acetonitrile, 5 mmol; H_2O_2, 5 mmol; temperature, 80 °C; time, 5 h)

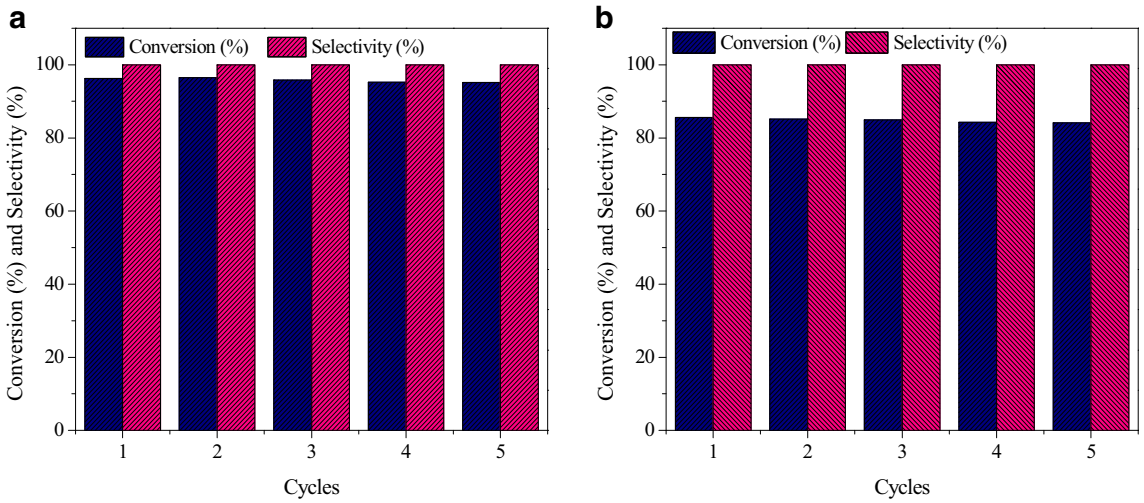

Fig. 11 The reusability of the spinel catalysts ($NiAl_2O_4$ NSPs and $NiAl_2O_4$ NPLs samples) for the catalytic oxidation of benzyl alcohol into benzaldehyde

the catalysts. The reusability of the catalyst for the liquid-phase oxidation of benzyl alcohol into benzaldehyde was evaluated, and the results are shown in Fig. 11. For the reusability study purpose, the spinel $NiAl_2O_4$ NSPs and $NiAl_2O_4$ NPLs sample catalysts were filtered off from each run, washed several times with ethanol, dried at 110 °C in an air oven for 1 h, and checked for five consecutive runs under the identical conditions. During the five runs investigated, the conversion of benzyl alcohol into benzaldehyde was in the range from 96.25 to 95.13 % for the $NiAl_2O_4$ NSPs sample (Fig. 11a), indicating that this catalyst displays good reproducibility and stability. Interestingly, the formation of benzoic acid was not detected. However, it was observed that the conversion of benzyl alcohol into benzaldehyde was in the range from 86.84 to 84.15 % for the $NiAl_2O_4$ NPLs sample (Fig. 11b). Since the spinel $NiAl_2O_4$ nanocatalyst is able to oxidize benzyl alcohol into benzaldehyde with high activity, highly recyclable, remarkably stable, and environmental friendly, they are promising candidates for the industrial and technological applications [48, 49].

3.9.5 Proposed Catalytic Oxidation Reaction Mechanism

In the proposed catalytic oxidation reaction mechanism for $NiAl_2O_4$ catalyst, the solvent CH_3CN can activate oxidant H_2O_2 by forming a perhydroxyl anion, OOH^-, to generate an intermediate peroxycarboximidic acid. It is well known that the formed intermediate peroxycarboximidic acid is a good oxygen transfer agent. The $NiAl_2O_4$ catalyst reacts with the H_2O_2 molecule to form Ni–OOH^- as an initiation step in this reaction. This perhydroxyl species, which are formed on the surface of the catalyst, will then oxidize the alcohol substrates. The benzyl alcohol and the H_2O_2 dissolve in CH_3CN, which activate H_2O_2 to OOH^- anion, forming Ni–OOH^- species [50]. This account revealed that the OH group of benzyl alcohols interacts with the Ni^{2+} ion. The contact of the OH group with the Ni^{2+} ions in $NiAl_2O_4$ is also clear by the adsorption of phenyl ring on the catalyst. However, the $NiAl_2O_4$ catalyst surface gets regenerated by the action of H_2O_2, which leads to desorption of the carbonyl product (benzaldehyde), thus favoring further oxidation. In addition, H_2O_2 has been proved to be a very efficient and environmentally friendly oxidant, since the product is only carbonyls [46, 47]. Usually, the catalytic oxidation of benzyl alcohol produces a mixture of carbonyls and carboxylic acids. However, carboxylic acid is not obtained in the present study. Therefore, the heterogeneous catalyst was found to be highly selective [51].

4 Conclusions

Spinel $NiAl_2O_4$ NSPs and $NiAl_2O_4$ NPLs have been successfully synthesized using MCM and CCM techniques, respectively, using urea as the fuel without any other solvent, surfactant, and catalyst. MCM approach is extremely facile and offers an inexpensive method for the preparation of nanostructured functional materials than CCM route. Powder XRD, FT-IR, EDX spectra, SAED, HR-SEM, and HR-TEM results showed that the as-prepared samples were pure phase spinel $NiAl_2O_4$ nanosphere and nanoplatelet-like particle morphologies with good crystalline nature prepared using MCM and CCM, respectively, without any other secondary phase impurity. The calculated optical band gap value of $NiAl_2O_4$ NSPs is 3.41 eV, which is higher than that of the $NiAl_2O_4$ NPLs sample (3.08 eV), due to the smaller particle size. The relatively lower M_s (49.16×10^{-3} emu/g) of $NiAl_2O_4$ NPLs shows that it is weak ferromagnetic in

nature, and the high M_s (73.42 $\times$ 10^{-3} emu/g) of $NiAl_2O_4$ NSPs confirms its ferromagnetic behavior. It was found that the $NiAl_2O_4$ NSPs sample shows higher conversion (96.25 %) than $NiAl_2O_4$ NPLs (84.15 %). Moreover, the MCM approach provides a simple and convenient method for preparing the transition spinel metal oxides. The synthetic route can be further used for the synthesis of other nanometal oxides.

References

1. Baykal, A., Deligoz, H., Sozeri, H., Durmus, Z., Toprak, M.S.: J. Supercond. Nov. Magn **25**, 1879 (2012)
2. Karaoglu, E., Baykal, A.: J Supercond. Nov. Magn **27**, 2041 (2014)
3. Amir, Md., Sertkol, M., Baykal, A., Sozeri, H.: J Supercond. Nov. Magn **28**, 2447 (2015)
4. Genc, F., Unal, B., Baykal, A., Sozeri, H.: J Supercond. Nov. Magn **28**, 1055 (2015)
5. Amir, Md., Baykal, A., Guner, S., Sertkol, M., Sozeri, H., Toprak, M.: J Inorg. Organomet. Polym **25**, 747 (2015)
6. Amir, Md., Baykal, A., Sertkol, M., Sozeri, H.: J Inorg. Organomet. Polym **25**, 619 (2015)
7. Guner, S., Amir, Md., Geleri, M., Sertkol, M., Baykal, A.: Ceram. Int **41**, 10915 (2015)
8. Amir, Md., Unal, B., Shirsath, S.E., Geleri, M., Sertkol, M., Baykal, A.: Superlatt. Microstruct **85**, 747 (2015)
9. Gozüak, F., Koseoglu, Y., Baykal, A., Kavas, H.: J. Magn. Magn. Mater **321**, 2170 (2009)
10. Koseoglu, Y., Baykal, A., Gozuak, F., Kavas, H.: Polyhedron **28**, 2887 (2009)
11. Manikandan, A., Durka, M., Arul Antony, S.: J Supercond. Nov. Magn **28**, 209 (2015)
12. Manikandan, A., Durka, M., Arul Antony, S.: J Supercond. Nov. Magn **27**, 2841 (2014)
13. Manikandan, A., Sridhar, R., Arul Antony, S., Ramakrishna, S.: J. Mol. Struct **1076**, 188 (2014)
14. Manikandan, A., Durka, M., Seevakan, K., Arul Antony, S.: J Supercond. Nov. Magn **28**, 1405 (2015)
15. Manikandan, A., Arul Antony, S., Sridhar, R., Bououdina, M.: J. Nanosci. Nanotechnol **15**, 4948 (2015)
16. Manikandan, A., Durka, M., Arul Antony, S.: Adv. Sci. Eng. Med **7**, 33 (2015)
17. Manikandan, A., Hema, E., Durka, M., Seevakan, K., Alagesan, T., Arul Antony, S.: J Supercond. Nov. Magn **28**, 1783 (2015)
18. Han, Y.S., Li, J.B., Ning, X.S., Chi, B.: J. Am. Ceram. Soc **88**, 3455 (2005)
19. Fonseca, R.L., Gonzalez, C.J., Rivas, B., Ortiz, J.I.G.: Appl. Catal. A **437**, 53 (2012)
20. Li, G., Hu, L., Hill, J.M.: Appl. Catal. A **301**, 16 (2006)
21. Cesteros, Y., Salagre, P., Medina, F., Sueiras, J.E. Chem. Mater **12**, 331 (2000)
22. Cui, H., Zayat, M., Levy, D.: J. Non-Cryst. Solids **351**, 2102 (2005)
23. Seo, J., Youn, M., Cho, K., Park, S., Lee, S., Lee, J., Song, I.: Korean J. Chem. Eng **25**, 41 (2008)
24. Hosseini, S.A., Niaei, A., Salari, D., Nabavi, S.R.: Ceram. Int **38**, 1655 (2012)
25. Valan, M.F., Manikandan, A., Arul Antony, S.: J. Nanosci. Nanotechnol **15**, 4580 (2015)
26. Valan, M.F., Manikandan, A., Arul Antony, S.: J. Nanosci. Nanotechnol **15**, 4543 (2015)
27. Manikandan, A., Arul Antony, S.: J Supercond. Nov. Magn **27**, 2725 (2014)
28. Manikandan, A., Durka, M., Arul Antony, S. J Inorg. Organomet. Polym **25**, 804 (2015)
29. Manikandan, A., Durka, M., Arul Antony, S.: J. Inorg. Organomet. Polym. **25**, 1019 (2015)
30. Manikandan, A., Durka, M., Arul Antony, S.: J Supercond. Nov. Magn **28**, 2047 (2015)
31. Meyer, F., Hempelmann, R., Mathurband, S., Veith, M.: J. Mater. Chem **9**, 1755 (1999)
32. Manikandan, A., Saravanan, A., Arul Antony, S., Bououdina, M.: J. Nanosci. Nanotechnol **15**, 4358 (2015)
33. Chinnaraj, K., Manikandan, A., Ramu, P., Arul Antony, S., Neeraja, P.: J Supercond. Nov. Magn **28**, 179 (2015)
34. Jeevanandam, P., Koltypin, Y., Gedanken, A.: Mater Sci. Eng. B **90**, 125 (2002)
35. Bayal, N., Jeevanandam, P.: J. Alloys Compd **516**, 27 (2012)
36. Wang, S.F., Gu, F., Lu, M.K., Cheng, X.F., Zou, W.G., Zhou, G.J., Wang, S.M., Zhou, Y.Y.: J. Alloys Compd **394**, 255 (2005)
37. Bai, H., Liu, Z., Sun, D.D.: Int. J. Hydrogen Energy **37**, 13998 (2012)
38. Schmidt, T., Lischka, K., Zulehner, W.: Phys. Rev. B **45**, 8989 (1992)
39. Sendi, R.K., Mahmudm, S.: Appl. Surf. Sci **258**, 8026 (2012)
40. Bhargava, R., Sharma, P.K., Dutta, R.K., Kumar, S., Pandey, A.C., Kumar, N.: Mater. Chem. Phys **120**, 393 (2010)
41. Shen, Y., Li, W., Li, T.: Mater. Lett **65**, 2956 (2011)
42. Ichiyanagi, Y., Kimishima, Y., Yamada, S.: J. Magn. Magn. Mater **272**, E1245 (2004)
43. Bhatt, A.S., Bhat, D.K., Tai, C., Santosh, M.S.: Mater. Chem. Phys **125**, 347 (2011)
44. Albuquerque, A.S., Tolentino, M.V., Ardisson, J.D., Moura, F.C., Mendonca, R., Macedo, W.A.: Ceram. Int **38**, 2225 (2012)
45. Hankare, P.P., Kamble, P.D., Maradur, S.P., Kadam, M.R., Sankpal, U.B., Patil, R.P., Nimat, R.K., Lokhande, P.D.: J. Alloys Compd **487**, 730 (2009)
46. Ali, S.R., Chandra, P., Latwal, M., Jain, S.K., Bansal, V.K., Singh, S.P.: Chin. J. Catal **32**, 1844 (2011)
47. Ma, C.Y., Cheng, J., Wang, H.L., Hu, Q., Tian, H., He, C., Hao, Z.P.: Catal. Today **158**, 246 (2010)
48. Seo, J.G., Youn, M.H., Park, S., Park, D.R., Jung, J.C., Chung, J.S., Song, I.K.: Catal. Today **146**, 44 (2009)
49. Loginova, E., Cosandey, F., Madey, T.E.: Surf. Sci **601**, L11 (2007)
50. Boudreau, M.D., Beland, F.A.: J Environ. Sci. Health Part C **24**, 103 (2006)
51. Hema, E., Manikandan, A., Karthiga, P., Durka, M., Arul Antony, S., Venkatraman, B.R.: J Supercond. Nov. Magn **28**, 253 (2015)